A Flux Scale for Southern Hemisphere 21cm EoR Experiments

Daniel C. Jacobs[1], Aaron R. Parsons[2], James E. Aguirre[3], Zaki Ali[2], Richard F. Bradley[4,5,6], Chris L. Carilli[7], David R. DeBoer[8], Matthew R. Dexter[8], Nicole E. Gugliucci[5], Pat Klima[5], Dave H. E. MacMahon[8] Jason R. Manley[9], David F. Moore[3], Jonathan C. Pober[2], Irina I. Stefan[10], William P. Walbrugh[9]

ABSTRACT

We present a catalog of broad-band spectral measurements from the Donald C. Backer Precision Array for Probing the Epoch of Reionization (PAPER) in South Africa observed in July and September of 2011. In order to reduce the impact of beam calibration, which proves to be a difficult endeavor for transit telescopes such as PAPER, on the determination of source spectra, we have focused on calibrating sources in a narrow declination range. Since each source follows a nearly identical path through the primary beam, this restriction allows beam calibration to be nearly eliminated as a source of error, yielding a dramatic improvement in the accuracy of source spectra measured in the 100–200-MHz band that is receiving renewed attention by experiments seeking to measure 21cm emission from the Epoch of Reionization (EoR). Based on the variation in our data and the estimated error in the absolute flux scale we bootstrap from multiple bright sources, we estimate PAPER measurements of sources above XXX Jy to be accurate to 3.2%. When combined with catalog data at other frequencies, these data constrain parameters of a power-law model for flux density with an uncertainty of 2.4%. This accuracy is limited by the uncertainty in the catalog measurements we use to estimate an absolute flux scale, and represents an order of magnitude improvement over previous measurements in this band. Comparing with prior measurements, 45 out of 58 sources observed are found to confirm and refine a power-law model for flux density.

[1]School of Earth and Space Exploration, Arizona State U., Tempe, AZ

[2]Astronomy Dept., U. California, Berkeley, CA

[3]Dept. of Physics and Astronomy, U. Pennsylvania, Philadelphia, PA

[4]Dept. of Electrical and Computer Engineering, U. Virginia, Charlottesville, VA

[5]National Radio Astronomy Obs., Charlottesville, VA

[6]Dept. of Astronomy, U. Virginia, Charlottesville, VA

[7]National Radio Astronomy Obs., Socorro, NM

[8]Radio Astronomy Lab., U. California, Berkeley, CA

[9]Square Kilometer Array, South Africa Project, Cape Town, South Africa

[10]Cavendish Lab., Cambridge, UK

This includes Pictor A, which provides a key flux reference for PAPER's EoR power spectrum analysis.

Subject headings: dark ages, reionization, first stars — catalogs — instrumentation: interferometers

1. Introduction

Numerous radio telescopes are now exploring the prospects for using measurements of highly redshifted 21cm emission to inform our understanding of cosmic reionization in the redshift range $6 < z < 12$, corresponding to radio frequencies below 200 MHz (see reviews in Furlanetto et al. 2006; Morales & Wyithe 2010; Pritchard & Loeb 2012). These include telescopes aiming to measure the global temperature change of 21cm emission during the Epoch of Reionization (EoR), such as the Compact Reionization Experiment (CoRE) and the Experiment to Detect the Global EoR Signature (EDGES; Bowman & Rogers 2010), and interferometers aiming to measure the power spectrum of 21-cm EoR emission, such as the Giant Metre-wave Radio Telescope (GMRT; Paciga et al. 2011, 2013)[1], the LOw Frequency ARray (LOFAR; Yatawatta et al. 2013)[2], the Murchison Widefield Array (MWA; Bowman et al. 2012; Tingay et al. 2013))[3], and the Donald C. Backer Precision Array for Probing the Epoch of Reionization (PAPER; Parsons et al. 2010; **?**)[4].

As such, there has been a renewed interest in the spectral and spatial variation of foreground emission in the 100–200 MHz frequency band that covers the $z = 6$–13 redshift range expected to encompass reionization (**?**). In particular, the spectral properties of extra-galactic point-sources are important both because they are valuable calibration references and because they are strong foreground emitters that must be removed from 21-cm EoR measurements. With the sparse availability of measured foreground properties in the 100–200-MHz frequency band over large areas of the sky (**?**), continued foreground characterization is a vital step en route to any 21-cm EoR detection. At these low frequencies the Southern sky is much less well known than the North, with catalog source fluxes at 150MHz being inaccurate at the 20% level for $\delta < -20^\circ$(XXX cite). Both PAPER and the MWA are located in the southern hemisphere at radio-quiet reserves being prepared for the upcoming Square Kilometer Array, and hence, the most extensive surveying work is now being conducted by the EoR experiments themselves (Jacobs et al. 2011; Williams et al. 2012).

One significant complication to improving the state of affairs in foreground characterization is that many 21cm EoR experiments, including LOFAR in the northern hemisphere, and PAPER and

[1] `http://gmrt.ncra.tifr.res.in/`

[2] `http://www.lofar.org/`

[3] `http://www.mwatelescope.org/`

[4] `http://eor.berkeley.edu/`

MWA in the southern hemisphere, are designed for drift-scan observations. This design decision has largely been driven by the simplicity and cost-effectiveness of phased and/or correlated dipoles for achieving the aggressive sensitivity requirements for measuring the 21cm power spectrum of reionization (XXX cite). Adding to the challenge, these telescopes cover much wider fields of view ($> 10^\circ$) and bandwidths ($\sim 100\%$ fractional) than traditional dish telescopes. Because they do not physically point, flux calibration for such arrays relies heavily on an accurate model of the primary beam response to correct for an the apparent flux scale that varies across the sky. This direction dependent gain is currently uncertain to 10% or higher (Pober et al. 2012), and comprises a large fraction of the 20% difference between current telescopes (Jacobs et al. 2013).

In this paper, we set out to significantly improve the accuracy of spectral measurements between 100–200 MHz for a set of bright sources in the declination range XXX to XXX that are of particular value for southern-hemisphere 21cm EoR experiments such as PAPER and the MWA. Using the fact that, for this restricted declination range, sources transit through a nearly identical primary beam response pattern, we are able to avoid one of the most debilitating source of error in these measurements: the primary beam. In §**??** we describe our approach for measuring source spectra with drift-scan observations and deriving an absolute flux scale from catalog data. In §4 we detail the instrumental setup, observations and analysis method followed. In §5 we compare the spectra with available data. We conclude in §6.

2. Background

Historically, the best EoR band data were by Slee (1995) with Culgoora Circular Array[5] and various higher frequency measurements with Parkes. These data are typically uncertain to 20% or higher and provide little coverage of the EoR band beyond a single narrow-band data point.

More recent surveys include narrow-band surveys by the GMRT and Mauritius, a deep survey of the region near Hydra A by the 32 antenna MWA prototype Williams et al. (2012) and a wide field survey by PAPER, also with 32 elements Jacobs et al. (2011). Several sub-channels were provided in the Williams catalog, though with 60-80% error bars —large compared to the 30% uncertainty on their wide band measurements. The latter cover the band and spatial scales relevant to EoR measurements but are limited by the accuracy of the primary beam (Jacobs et al. 2013).

A method for decoupling uncertain fluxes from the uncertain beam has been described by Pober et al. (2012). In simulation the method was able to achieve 3 to 10% accuracy in measuring the primary beam, depending on the number of antennae and other variables. The Pober method emphasized the need for many repeated measurements of each alt-az pointing. Further investigation is under way to improve and implement this method and would be greatly aided by the availability of precise flux measurements unaffected by primary beam uncertainty.

[5]Known during daylight hours as Culgoora Radio Heliograph

This paper reports a set of flux measurements where a primary beam model has not been used to estimate the flux, but instead are directly calibrated to a single calibrator making the track through the beam.

EoR measurements in the southern sky have focused on the coldest regions where galactic foregrounds are minimal. With the majority of possible observing time falling on RA=4h,Dec=-30. The brightest and least-resolved calibrator in this region is Pictor A (5h19m49.1 -45d46m45.0). Pictor A is a nearby FR-II type radio galaxy similar to Cygnus A. At ∼400Jy Pictor is bright and sufficiently distant from other bright sources to make it eminently suitable as both a phase and flux calibrator. Its apparent size of ∼8′is smaller than the scales being probed by current EoR instruments , making resolution effects, making it suitable for precision calibration. However, like most other sources, precise flux measurements in the EoR band are not available. The current best EoR band measurement is uncertain to 12% and appears to imply spectral flattening in the EoR band (Perley et al. 1997).

Establishing an accurate spectrum for Pictor A is of particular importance for PAPER — a dedicated EoR experiment that employs drift-scanning, dual-polarization dipole antennas tuned for efficient operation over a 120–170-MHz band. PAPER is located in the South African Karoo desert on the Square Kilometer Array South Africa (SKA-SA) reserve, 100km north of the small town of Carnarvon. The PAPER array has grown from 16 elements deployed in early 2009 to a 64-element imaging array in 2011 (see Figure 2). Since November 2011 it has been arranged in a maximally redundant grid configuration to make deep power spectral integrations (**?**). Though highly sensitive as a power spectrum instrument, the maximally redundant array has a broad point spread function in the image domain. This severely limits the number of sources which may be used for flux calibration. Drift scanning across the sky with a 45°FWHM primary beam there are very few unresolved, bright sources which are far from the galactic plane. Pictor A is bright and well enough separated from other emission to dominate the visibilities for a good fraction of the EoR observing season, making it an ideal flux calibrator.

3. Approach

Given the large uncertainties in the literature, and the necessity for PAPER power-spectrum analysis to use Pictor A for flux calibration, we felt it prudent to examine Pictor A directly. In this section, we describe how we use PAPER in its imaging configuration to measure Pictor A and a selection of known, bright sources in a 5°strip centered on -45°.

In **?** several limitations were identified that exasperated the primary beam uncertainty. First, in imaging each source flux is measured at just a few points in the primary beam. As errors tend to vary across the beam, the uncertainty will tend to vary between sources. Here we have averaged over all possible positions making the uncertainty a function of the net uncertainty in the beam, and stabilizing the source-to-source variations in error bars. The second limitation, identified in

Williams et al. (2012), was the increase of uncertainty towards the edge of the beam. To minimize our sensitivity to both beam and noise uncertainty, we weight the source track by an additional factor of the primary beam model.

As PAPER is a drift scan instrument, each declination δ describes a distinct cut through the primary beam. These cuts provide a detailed measurement of the primary beam relative to the peak of the trace, however, a model $g(\delta)$ is still required to calibrate between declinations. This model will be effective over a range of declinations, but will diverge at some rate depending on the accuracy with which the model describes the slope. As an estimate of the extrapolated beam amplitude we fit the slope of our Pictor A source track and compute the amplitude extrapolated over our fiducial stripe width of 5°.

$$B = dB/dtdt/\theta\Delta\theta$$

Comparing this with the simulation in Figure 1, we find that the model predicts the 5°extrapolation to better than 2% even into the more uncertain areas far from zenith. The RMS difference for the central 15°of the track is 1.5%. From this we conclude that, as long as we constrain our extrapolations to ±5°around Pictor A, we will have negligible beam area.

We choose sources from the Molonglo Reference Catalog (Large et al. 1981, MRC) that are within 5°in declination of a common calibrator (J2331-416) and have a flux extrapolated from 408MHz greater than 10Jy assuming a power law spectral index of -1.[6] This selection contains 62 sources in a narrow stripe that passes through the majority of the southern EoR fields, much of the galaxy and Centaurus A. This stripe in the broader context of the galactic plane is shown in Figure 18. A list of these sources is given in Table **??**.

For these sources, spectral data measured below 2 GHz were compiled from the NASA/IPAC Extragalactic Database (NED) [7]. Cross-matching radio sources between bands is made difficult by changes in resolution, spectral curvature, and resolved multi-scale structure. For a small number of sources these problems can be ameliorated by inspection of the spectra, source names, coordinates, and originating publications. However for a large sample of sources this becomes unwieldily and prone to error. Thus for the larger number of samples we make use of the Vollmer et al meta-catalog which takes pains to match multi-wavelength observations (Vollmer et al. 2010).

The spectra reported here are measured by beam-forming, phasing the visibilities to the target location, and summing to produce a dynamic spectrum. The spectrum is then isolated from neighboring sources by filtering and averaged in the time domain. This time average is weighted

[6]Most radio sources in this band have power law spectra $S(\nu) = \left(\frac{\nu}{\nu_0}\right)^{\alpha}$.

[7]`http://ned.ipac.caltech.edu/`

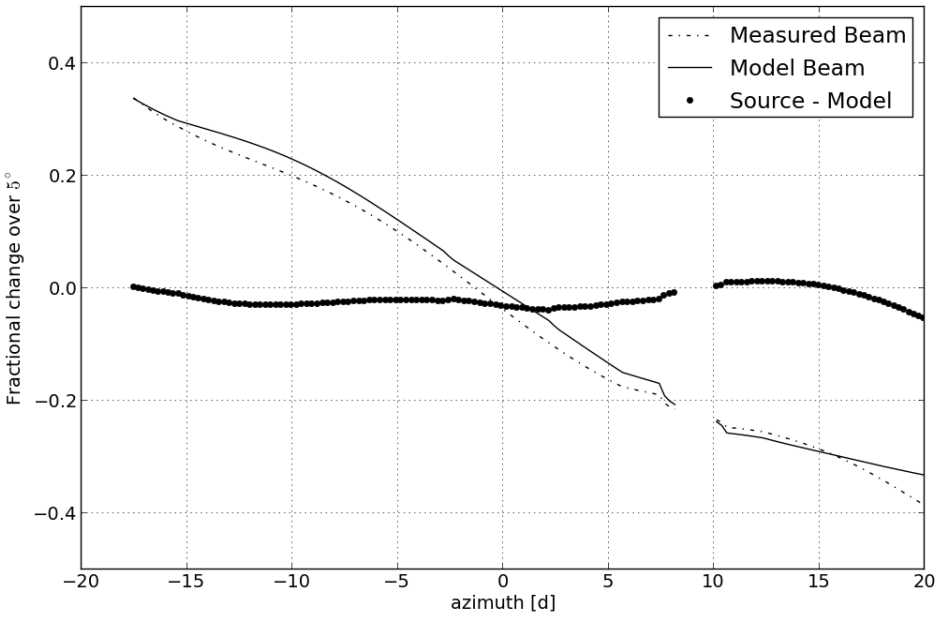

Fig. 1.— The beam is well along a declination cut but beam formed source tracks. Here we measure the beam, as extrapolated by fitting a slope (dotted), and compare with the beam model (solid). The difference (circles) is never larger than ∼1%. Thus we conclude that the beam slope is locally well modeled and our beam model is suitable for extrapolation over ∼5°scales.

by an additional factor of the PAPER's primary beam response (**?**).

$$S_{\rm est} = \frac{\sum_t B_M S_p}{\sum_t B_M^2} \tag{1}$$

$$= \frac{\sum_t B_M B}{\sum_t B_M^2} S \tag{2}$$

$$\tag{3}$$

which is an effective approximation of inverse-variance weighting. The pre factor in Eq 3 is identical for sources at the same declination, and as we found above, diverges slowly from the model in the 10°declination stripe. We estimate this spectral dependent gain for a calibrator (J2331-416) fitting a spectral index model to the well-defined data points below 2GHz. This removes an overall offset.

Finally we average the spectra from a resolution of 400kHz to 10MHz bins, taking the standard deviation within these bins for an estimate of the uncertainty.

At this point we have a set of spectra that have been calibrated relative to each other to the best of our ability. Now they must be put on a global flux scale. We also have only a limited estimate of our error from our intra-channel rms. To address both points we fit for a global flux scale that incorporates data from many catalogs. These catalogs have all been set, as best as possible, to the Baars et al scale. Using a Bayesian analysis we compute the variation in the flux scale implied by comparing many sources to prior catalog. By including sources from across the declination range,the variation in this flux scale fit estimates the overall uncertainty in flux resulting from primary beam or prior catalog uncertainty. So though the final scale is calibrated to the Baars scale as extrapolated beyond its defined band, the error on the flux scale fully encapsulates the error resulting from this extrapolation.

4. Data Reduction

4.1. Observations

Measurements are derived from observations using the east-west dipole arms of 64 PAPER antennas deployed in a minimum-redundancy imaging configuration (see Figure 2) at the Karoo Radio Observatory site in South Africa. A 100-MHz band from 100-200MHz was correlated with 2048 frequency channels and integrated for 10.7 seconds before visibilities were stored. Observations included here on July 4, 2011, running from JD2455748.17 to JD2455748.72. and October 17, 2011 running from JD2455852.2 to JD2455852.6. In both seasons two antennas were omitted owing to malfunctioning signal path. This 20 hour long combined dataset provides observations provides complete hour angle coverage for the entire 24 hours of Right Ascension. The July portion of the dataset comes from the same observing campaign described by Pober et al. (2013) and Stefan et al. (2012).

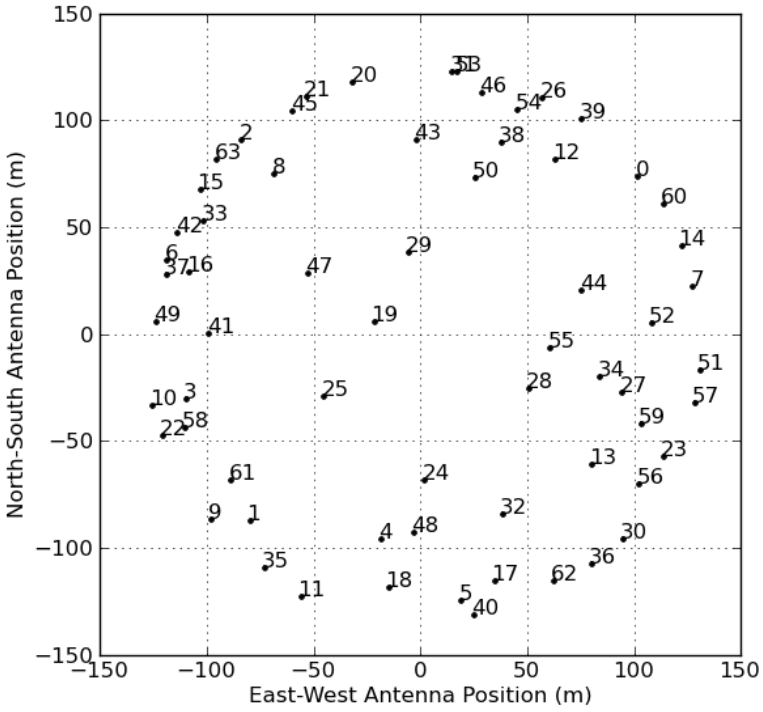

Fig. 2.— Antenna position in the 64-antenna, minimum-redundancy PAPER array configuration at the Karoo Radio Observatory site in South Africa used for these observations. Data was captured during July and October of 2011 on a single 'x' polarization over a band between 120 and 180 MHz.

4.2. Data Compression

In pre-processing, we use delay/delay-rate (DDR) filters (Parsons & Backer 2009) to identify radio-frequency interference (RFI) events, and as part of a data compression technique that reduces data volume by over a factor of 40. A more detailed description may be found in Appendix A of **?**, which uses the same compression method on PAPER power spectrum observations. Here we summarize the process.

First, we remove known RFI transmission bands and analog filter edges, and then flag outliers at 6σ to remove RFI events. Next, we suppress foreground emission by applying a DDR filter to remove delays and delay-rates within the horizon limit of a 300-m baseline (the maximum length of any PAPER baseline). We derive a second set of RFI flags by masking 4σ outliers in these residuals and apply these flags back to the unfiltered data. Finally, we compress the data by applying a DDR filter preserving emission within the horizon limit of a 300-m baseline, deconvolving to suppress flagging artifacts, and down-sampling the result in time/frequency domain to the critical Nyquist rate of the DDR filter. The result is that the 2048 original frequency channels become 203, and the 60 original time samples per 10-minute file become 14.

4.3. Per-Antenna Gain Calibration

Small gain variations between antennae and over time introduce significant systematic effects which degrade instrument performance. Temporal variations are dominated by changes in ambient temperature. Measurements of ambient temperature versus time near the balun amplifier of a fiducial antenna and near receiver amplifiers were used to divide out the predicted gain variation versus temperature that these amplifiers are known to exhibit. A predicted gain profile was derived using coefficients characterized in laboratory measurements (**?**) and confirmed in field measurements (**?**) of $H_{\rm balun} = -0.024$ dB/K, $H_{\rm recvr} = -0.045$ dB/K, and $H_{\rm cable} = -0.018$ dB/K for 150m-long cables. Because cable temperatures were not measured during these observations, the cable temperature was assumed to be the same as the measured balun temperature.

Matching of relative gains and phases between antenna was done by fitting a per-antenna complex gain to portions of data which have easily modeled sky. This calibration is only relative between antennae, absolute flux calibration comes after time and frequency averaging in §4.7. The antenna delays and amplitudes were found by fitting a point source visibility model to Centaurus A, Pictor A, and Fornax A. Each source is imperfectly modeled by a single point-source, but the solution differences are minimized by averaging over the three independent solutions. These same calibration solutions have been successfully applied in **?** and **?**. for power-spectrum analysis of foregrounds and imaging of Centaurus A, respectively.

4.4. Beamforming

Spectral time-series are computed by beam-forming to the selected sky locations. A beam is formed by phasing baselines to the desired location and summing over baselines longer than 20 wavelengths.

These complex spectra are then fringe rate filtered to remove spectrally smooth sources that deviate more than ±0.1mHz from the fringe rate of the source in question (Parsons & Backer 2009) (cf the LOFAR de-mixing approach Offringa et al. (2012)) producing a time dependent spectrum with minimal side lobes. This is then averaged in time, weighting by a model of the primary beam as discussed above. The result is equivalent to a very long earth rotation synthesis image with a single image pixel. The weighted contributions from each baseline are shown in Figure 3.When combined with the filtering it is a robust and simple method for measuring spectra of unresolved sources.

4.4.1. Compensation for Resolution Effects in Pictor A

The beam-forming method assumes the target is a point source. Our primary target, Pictor A, is slightly resolved by PAPER, and merits closer attention. Pictor A is a double-lobed radio galaxy with a main lobe separation of 7′. As we see in Figure 4, it is nearly unresolved by PAPER's 15′synthesized beam. However, given the high SNR of the observations, we see a 20% drop in flux on the longest (∼300m) baselines. We account for this by weighting baselines in the beamform step according to a model of structure observed by Perley et al. (1997) at 330MHz, which they found to be consistent with their more limited 74MHz images as well as the detailed high frequency maps. The normalized image is Fourier transformed and sampled at the desired uv spacing by spline interpolation. These samples are used to weight each baseline contribution in the baseline sum. The result is an estimate of the total integrated flux for Pictor A. Where the resolution is highest, at the top of the band, the correction is 3%. At the bottom of the band, where the resolution size has grown to 19′, the correction is only 0.6%. The resulting spectrum is shown in Figure 7a.

4.5. Bandpass Calibration

The resulting set of spectra were then calibrated to a model of J2331-416 to remove the residual bandpass due to the net effect of the primary beam as discussed in §3. J2331-416 [8] fit to measurements beolow 1GHz (**????**). was selected for its relatively high brightness, spectral smoothness and large quantity of available catalog data. Each source track has a slightly different sample profile resulting from different amounts of flagged data at each time and channel. To

[8]Here we set the spectrum to $S_{150} = 33$Jy, $\alpha = -0.76$

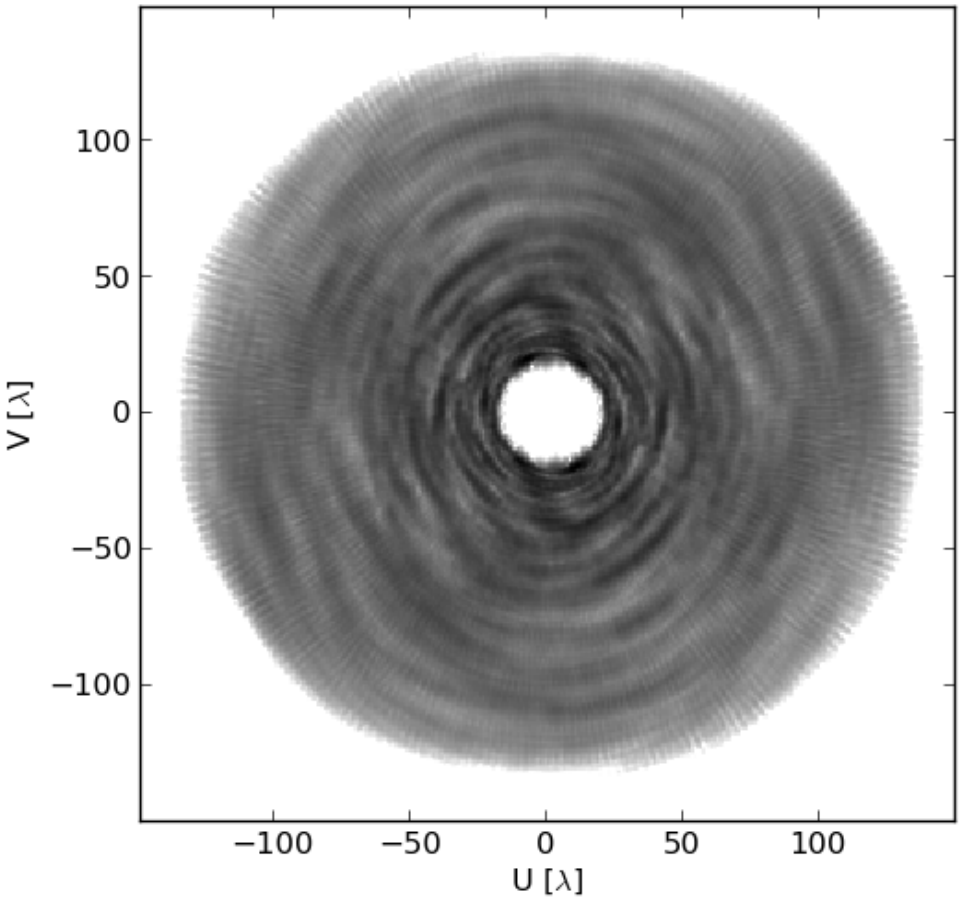

Fig. 3.— The effective uv coverage of a 10MHz-wide spectrum bin, showing the relative contributions of each baseline when beam-forming on Pictor over a 9.6 hour synthesis in the October observing session.
Not shown here are the weights interpolated from the Perley et al 330MHz map (Fig. 4) used to recover the total integrated flux of Pic which represent a few % change on the longest baselines.

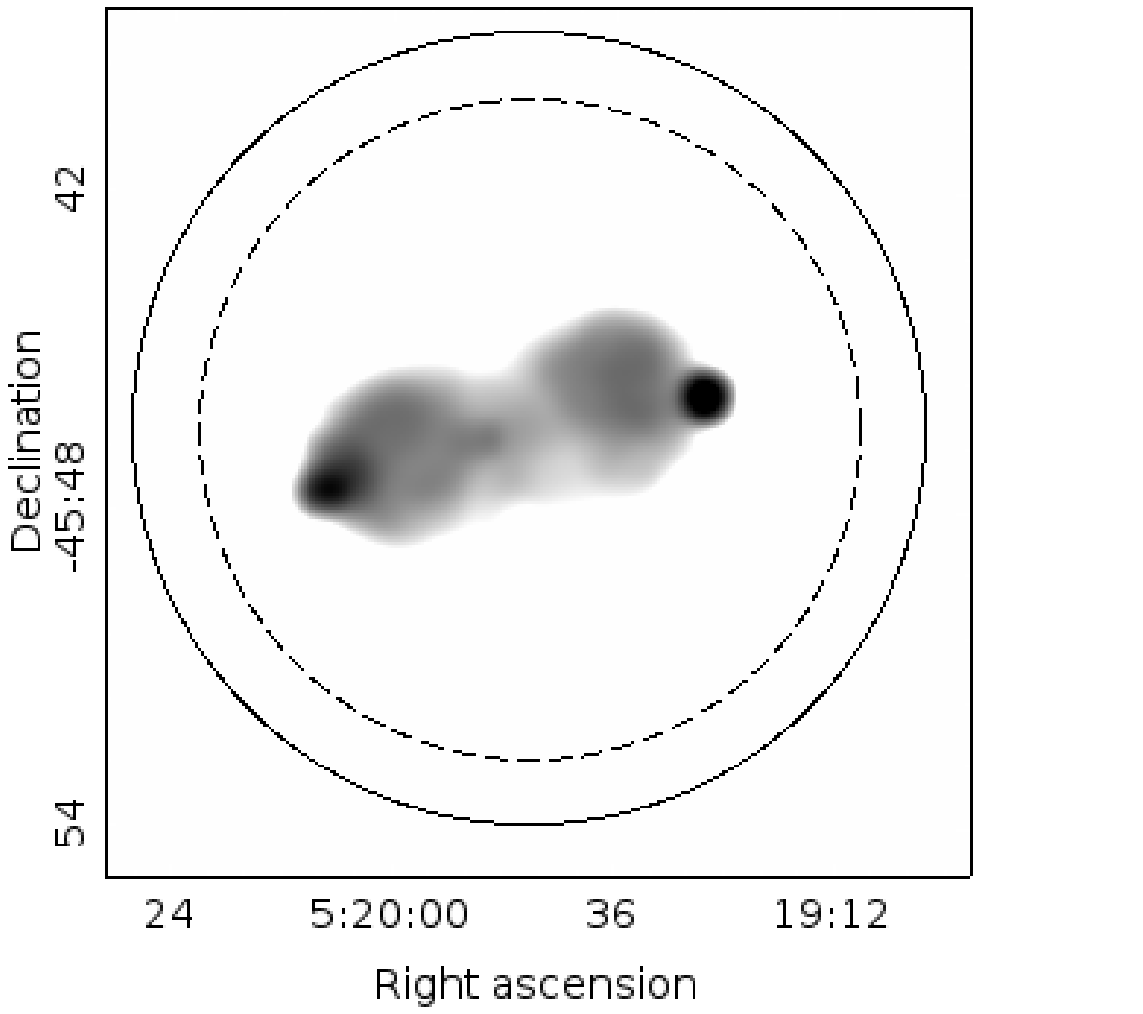

Fig. 4.— Pictor A imaged at 330MHz by the VLA (Perley et al. 1997). Black circle indicates PAPER resolution at the 150MHz, dashed, the resolution at 185MHz. To correct for the small residual structure in the PAPER measurements we resampled the Perley image to the PAPER resolution and estimated the relative contribution to each PAPER baseline. At the highest frequency this led to a 3% correction, at the lowest frequency, 0.6%.

account for these differences in the bandpass calibration we build a set of calibration tracks that match the tracks for each source. Calibration of each source then proceeds with an optimally matched calibration spectrum.

4.6. Fitting a Power-Law Model to Spectra

There is a variety of prior data at multiple wavelengths to which we want to calibrate and then compare our measurements. Our method for doing both of these steps is to assume a basic spectral model relating the different catalog data points and fit for spectral model and gain parameters.

We estimate spectral model parameters and flux calibration in a Bayesian way by calculating and marginalizing the posterior probability of the catalog and new PAPER data. This method offers improved repeatability by specifying a single objective function that represents the quality of the model fit and naturally defines the errors on the parameters (Hogg et al. 2010). See Mackay (2003) or Sivia & Skilling (2006) for more on Bayesian analysis methods and an excellent astrophysical example by Press (1997). In brief, measurement errors are related to parameter model errors via the likelihood, which we can calculate, and the posterior, which we cannot. However, the posterior is theoretically well sampled by a Markov Chain Monte Carlo sampler, which selects parameter values at random, computes the likelihood of the model given the data and noise model, and accepts or rejects the step based on an outside decision factor unrelated to the data.

Here we use the emcee sampler by Mackay (2003) et al to generate chains of parameter values. The best fit model is the median of all the sampled parameter sets, while the volume containing a well defined fraction of samples sets the confidence limits. The oft quoted "1σ" probability level corresponding to a gaussian distribution contains 65% of the samples. In practice the contours are not gaussian. Here we choose a slightly more conservative probability level of 76%

To model the relationship between different wavelengths we assume a single spectral index which is the prevailing spectral energy distribution at low frequencies, though curvature or other deviation from a power-law is not-uncommon.

When fitting models to the full catalog, we use the Vollmer et al catalog which has been optimally cross-matched at the expense of excluding more data points. Meanwhile, the gain fit used a small sample of sources with spectra which meet our calibration criteria: more precision data available, brighter than most sources in the sample and far from any possibly confusing areas of the sky. By limiting ourselves to a small number of sources we are able to go include catalog points by hand, to avoid making the error of falsely including erroneously matched data points but benefiting from some measurements not included.

4.7. Approximating an Absolute Flux Scale

At the output of the beam forming and bandpass calibration step, the flux scale is tied to a model fit tp the catalog values of J2331-416. The accuracy of this fit, and the implied uncertainty in the flux scale, limits the accuracy of the PAPER measurements.. To refine the flux scale and estimate our flux scale uncertainty, we bootstrap a single global flux scale correction factor using 5 sources selected for their brightness, spectral linearity and data availability[9]. To build a more complete spectral model we go beyond the data found in Vollmer et al, including all spectral measurements below 2GHz found in the NED database [10]. These catalog measurements are primarily by Parkes, and Molonglo with the best precision coming from the Wills fluxes at 538 and 634 MHz (when available). Where error bars are not given, we assume uncertainty of 25%.

Using the MCMC method we fit spectral index models to the catalog fluxes simultaneously with a global PAPER flux scale factor using an MCMC chain to calculate the log likelihood

$$\log \mathcal{L}_s = \sum_{\nu} \frac{(S^{\nu}_{\rm cat} - S_{150}\left(\frac{\nu}{150}\right)^{\alpha})^2}{2(\Delta S^{\nu}_{\rm cat})^2} + \frac{(g * S^{\nu}_{\rm PAPER} - S_{150}\left(\frac{\nu}{150}\right)^{\alpha})^2}{2(\Delta S^{\nu}_{\rm PAPER})^2} \tag{4}$$

$$\log \mathcal{L} = \sum_{s} \log \mathcal{L}_s \tag{5}$$

which samples the posterior probability of PAPER data ($SPAPER_{\nu}$) and catalog values ($Scat_{\nu}$) given a spectral index model for each source and a global flux scale factor (g) ($S^{\rm calibrated}_{\rm PAPER} = gS_{\rm PAPER}$). Marginalizing over the fitted flux scales, we find the resulting flux scale distribution function which is shown in Figure 6. The 76% confidence limit on this flux scale, relative to the J2331-413 calibration, is $-0.01^{+0.11}_{-0.17}$ dB, or a 3.24% multiplicative error on every calibrated PAPER measurement. These errors are added, in quadrature, to the errors in the PAPER spectra.

These calibrated spectra are plotted in Figures 8,9, & 10 and the data are listed in Table 1. The resulting Pictor A spectrum ranges in precision from 6.5% at 125MHz to 4.7% at 185MHz. At least half of this error is due to uncertainty in the flux scale.

4.8. Fitting Spectral Models

Finally we compare all of our calibrated spectra to catalog measurements. Our method will be to first establish a best fit model to existing data, then add the PAPER data to the fit, and assess the degree to which the PAPER data is supported by prior measurements, or the reverse the degree to which PAPER offers an improvement in our knowledge of the spectrum.

---

[9]Calibration sources: 2250-412,2331-416,2140-434,0007-446,0704-427

[10]`ned.ipac.caltech.edu`: Accessed 1 April 2013

To establish the baseline model, we fit a spectral model to catalog data from the spectrally and spatially cross-matched meta-catalog by Vollmer et al. (2010) using the (log) likelihood which assumes Gaussian measurement errors

$$\log \mathcal{L} = \sum_{\nu} \frac{\left(S_\nu - S_{150}\left(\frac{\nu}{150}\right)^{\alpha}\right)^2}{\Delta S_\nu} \tag{6}$$

We estimate the confidence interval of the resulting parameters as the boundary enclosing 76% of the samples. In the catalog we report both the upper and lower of these values for both parameters and plot the 2D contour to show the correlation of the two parameters. Many of these contours, the grey curves in Fig. 11, are classic banana plots, displaying a non-linear correlation between the parameters. In most cases the single contour adequately describes 2D posterior distribution.

Confidence contours for the complete set are shown in grey in Figs. 11 - 14. In general these are lower limits on the possible precision, as the Vollmer catalog emphasizes minimization of cross-match error but at the cost of excluding data points. The fit is then performed again with both PAPER and catalog data, shown in black on the same Figures. The values are given in Table 2, and illustrated in Figure **??**.

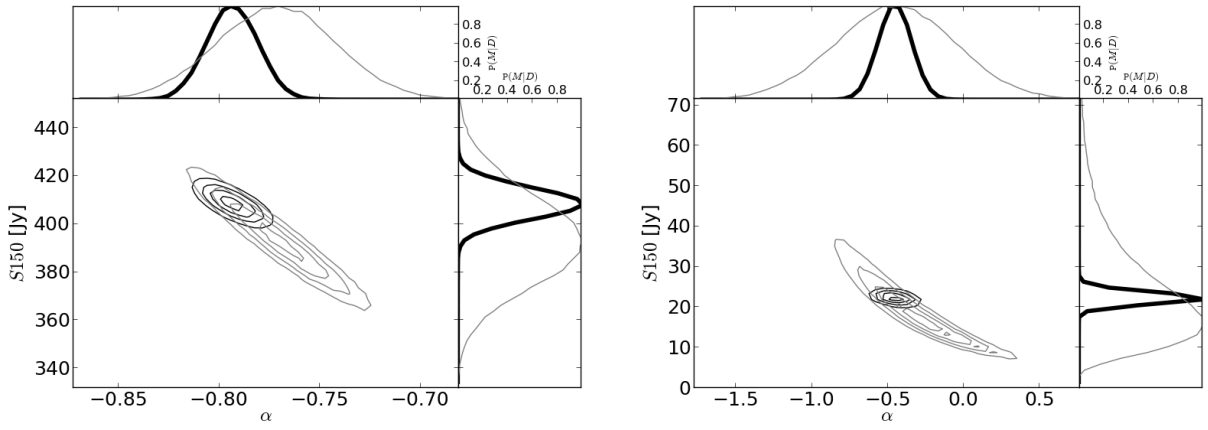

Fig. 5.— A more detailed view of the posterior probability distribution. On the left Pictor A, on the right 1556-466. Confidence contours range from 0.2 to 0.8. Compare with the contours for this source shown in Fig. 13. As above, grey for the fit to catalog data, black for joint catalog and PAPER fit.

5. Results and Discussion

In the 59 sources measured, four demonstrated poor convergence fitting a single spectral index to both the PAPER data and prior catalog data. In three cases[11] the Centaurus A/galactic plane region. Though the beam forming method provides relatively high dynamic range of ∼100:1 it is unable to distinguish between these sources and the bright diffuse Centaurus and galactic structure. The last source, 0008-421, was not detected by previous PAPER observations and exhibits flattening at higher frequencies, most likely due to synchrotron self-absorption (Jacobs et al. 2011) . The remaining 94% MCMC chains arrived at a stable posterior distribution. The spectral index parameters for these chains are given in table 2.

Inspecting the confidence contours we find that, for the vast majority ($\sim 75\%$), the PAPER measurements confirm the power law extrapolation from higher frequencies. The remaining 25% either A) have large PAPER error bars and therefore provide no new information or B) do not agree with the spectral index model. To understand where most measurements fall on this spectrum we numerically quantify the overall model improvement derived from the addition of the PAPER data as

$$\text{Improvement} = (\text{Precision increase})\,(\text{Catalog agreement}) \tag{7}$$

$$= \left(\frac{1}{Area(\text{PAPER})} - \frac{1}{Area(\text{Cat})}\right)(Area(\text{PAPER} \cap \text{Cat})) \tag{8}$$

We quantify the fit *precision increase* as the change in the contour figure of merit, defined as the inverse area of the confidence contour. Meanwhile, *catalog agreement* is the fraction of the PAPER confidence interval that overlaps the catalog confidence interval. Thus, for example, in a PAPER fit that overlaps the catalog confidence contour by 41% but increases in precision (confidence area shrinks) by a factor of 3, the resulting *improvement* will be 0.123.

In these sources, the improvement index ranges from a max of 6.9 to -0.022. 10% of sources showed negative improvement, suggesting that PAPER data have added to uncertainty (see Figure 16). 12% of sources have exactly zero improvement, which indicates that the PAPER data have pulled the fit far from the model preferred by the catalog data (see Fig. 17). The spectral models of these sources have not been included in Table 2. The remainder of the spectral fits are included for completeness, but given the range of quality found, particularly near the Galactic plane and Centaurus A, should be used with utmost caution.

However, the majority of source 78% have positive improvement index, indicating strong confirmation of the extrapolated spectrum (see Figures 11 - 14). Pictor A is in the middle of this group with an improvement of 0.39 —only 14 sources show stronger confirmation. The flux model is $S150 = 388 \pm 9.4$Jy, $\alpha = -0.77 \pm 0.02$. The combination of several independent PAPER data

[11] 1243-412,1247-401,1315-460

points near 150MHz with previous catalog measurements results in this estimated uncertainty of 2.4%. This uncertainty is dominated by agreement between the 2 Wills measurements near 600MHz which are accurate to 2% and the five PAPER measurements, which are accurate to 5%. This error estimate includes an estimate of accuracy of the overall flux scale, as well as the source-source variation due to primary beam errors.

6. Conclusion

Here we have provided a measurement of Pictor A with enough precision to confirm a highly linear spectral index between 150 and 600MHz. We then used the same filtered beam form method to measure the spectra of bright sources with similar primary beam response. This primary beam limit is based on our measurements of the primary beam along slices of constant declination.

The measurements provided here are the first, calibrated, broad-band spectra to cover the EoR band. Existing EoR band measurements are accurate to 20% implying a 40% uncertainty in the absolute power spectrum level. The Pictor A spectrum here is shown to be accurate to ∼5%, a factor of 5 improvement over previous measurements.

This uncertainty includes the variation in each PAPER measurement (∼1%), variation between sources and the errors resulting from extrapolating the Baars et al. (1977) scale beyond its original range. These last two are found simultaneously by fitting the spectral extrapolations of several flux calibrators at once and account for the the majority of the error. Though past measurements suggested the possibility of spectral curvature below 200MHz we have found no evidence for this. With these measurements we are able to confirm single spectral index model for Pictor between 120MHz and 600MHz.

A set of 61 verification sources were selected to be bright, previously cataloged and distributed over the full 24 hours of Right Ascension coverage but only within 5 degrees declination of Pictor A. Using a Bayesian analysis we conclude that most of these are consistent with previous measurements and provide useful new constraints. However, in a small remainder, the simple spectral model fails to adequately describe the data. In most cases the proximity to bright or extended structures implies side lobe contamination. Therefore, though we include the model parameters, they are not meant to be definitive, but provide confidence that the reported PAPER flux values are on the correct global scale.

Direct measurements of the Pictor A spectrum are key to correctly setting the flux scale of PAPER, MWA and future EoR experiments like the Hydrogen Epoch of Reionization Array (HERA). These spectra provide tighter constraints on many of the EoR band fluxes, while limiting the pernicious affect of primary beam uncertainty. Future work will use these fluxes to further refine the primary beam models of these experiments which is crucial to properly reconstructing both image and power spectrum flux.

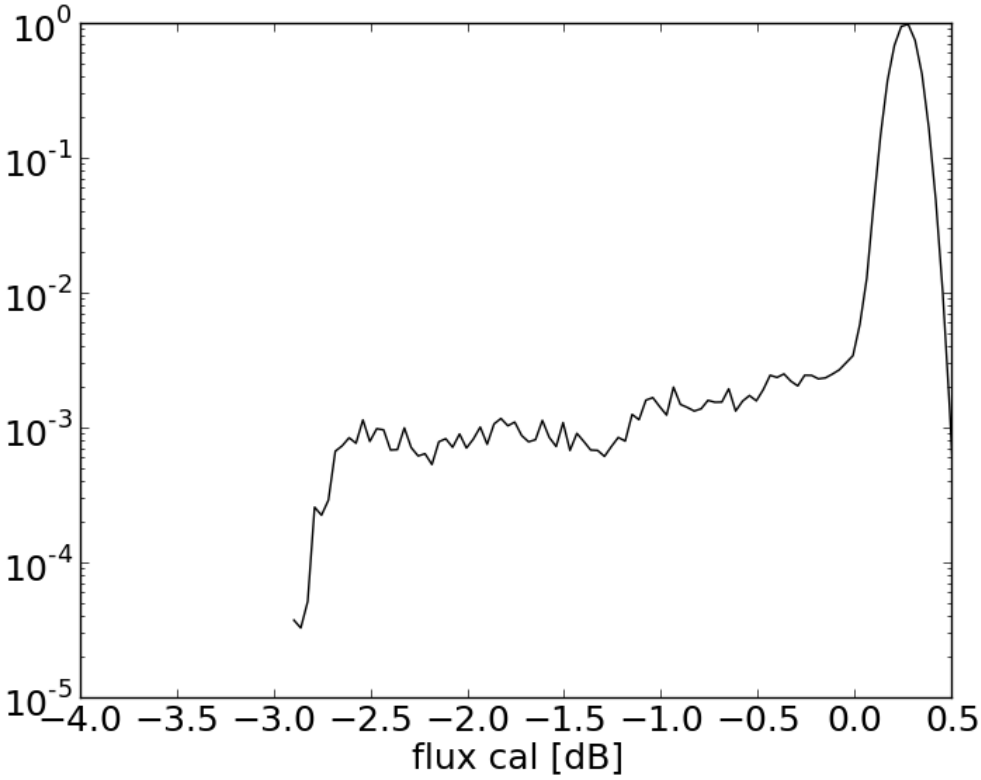

Fig. 6.— The marginalized PAPER flux scale factor posterior probability distribution function bootstrapped from the NED database listings for 2250-412,2331-416,2140-434,0007-446 and 0704-427 below 2GHz.

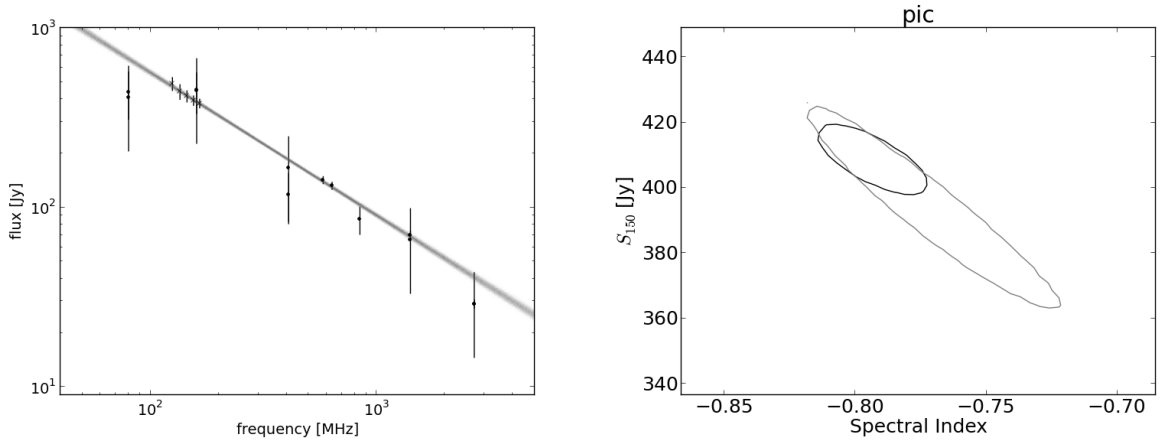

Fig. 7.— Using new PAPER results to constrain the spectrum of Pictor A. On the left, the PAPER Pictor A spectrum with 2σ error bars (x) and MCMC fits (grey cloud). Inset allows comparison between the 10MHz averaged points with the 403kHz points (grey). The oscillations in the PAPER spectrum are residual side lobe contamination from other sources and are well represented by the error bars. The most reliable prior measurements (dots) are those by Wills (1975) at 580MHz and 635MHz (Perley et al. 1997). The rest are from with Culgoora Slee (1995) or Parkes Otrupcek & Wright (1991) and have been set to the (extrapolated) Baars et al. (1977) scale by Kuehr et al. (1981). A sub-sample of MCMC fits are shown in blue. On the right, the grey contour indicates the 76% confidence interval for 150MHz flux and spectral index given the prior data. Black folds in the PAPER data.

Acknowledgements

The PAPER project is supported by the National Science Foundation (awards 0804508, 1129258, and 1125558), and a generous grant from the Mt. Cuba Astronomical Association.

This work makes use of]the "MCMC Hammer" emcee python library (Foreman-Mackey et al. 2012, `http://danfm.ca/emcee/`) and the NASA/IPAC Extragalactic Database (NED) which is operated by the Jet Propulsion Laboratory, California Institute of Technology, under contract with the National Aeronautics and Space Administration.

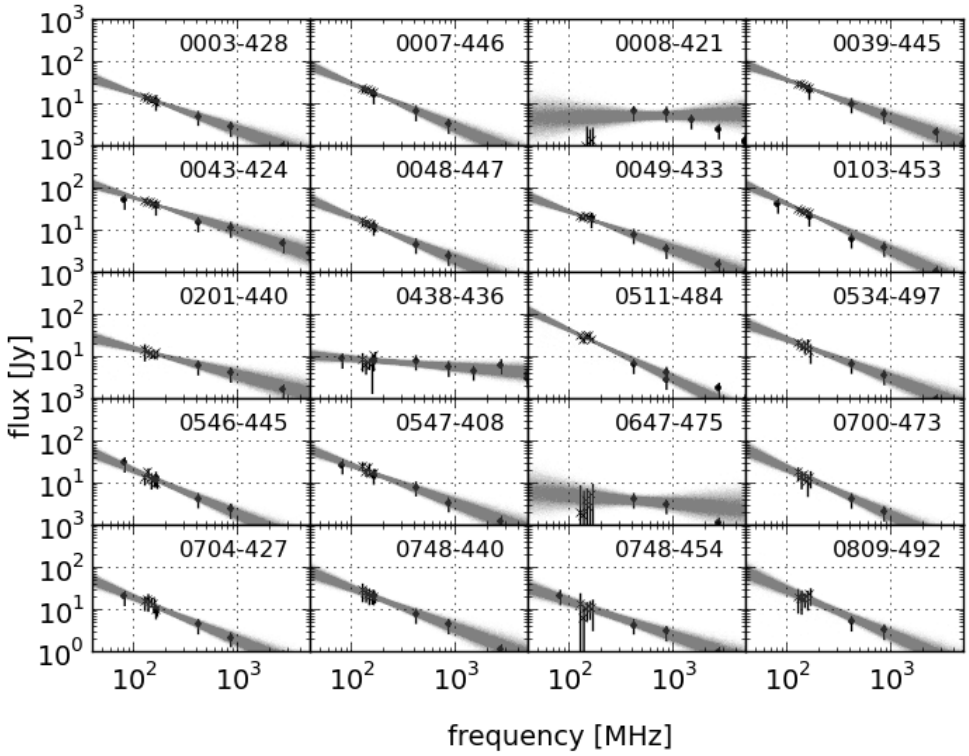

Fig. 8.— PAPER spectra of 16 sources compared against existing data out of Vollmer et al. (2010) between 40MHz and 2GHz, otherwise as described in Figure 7.. Sources used to bootstrap the flux calibration are noted with a *.

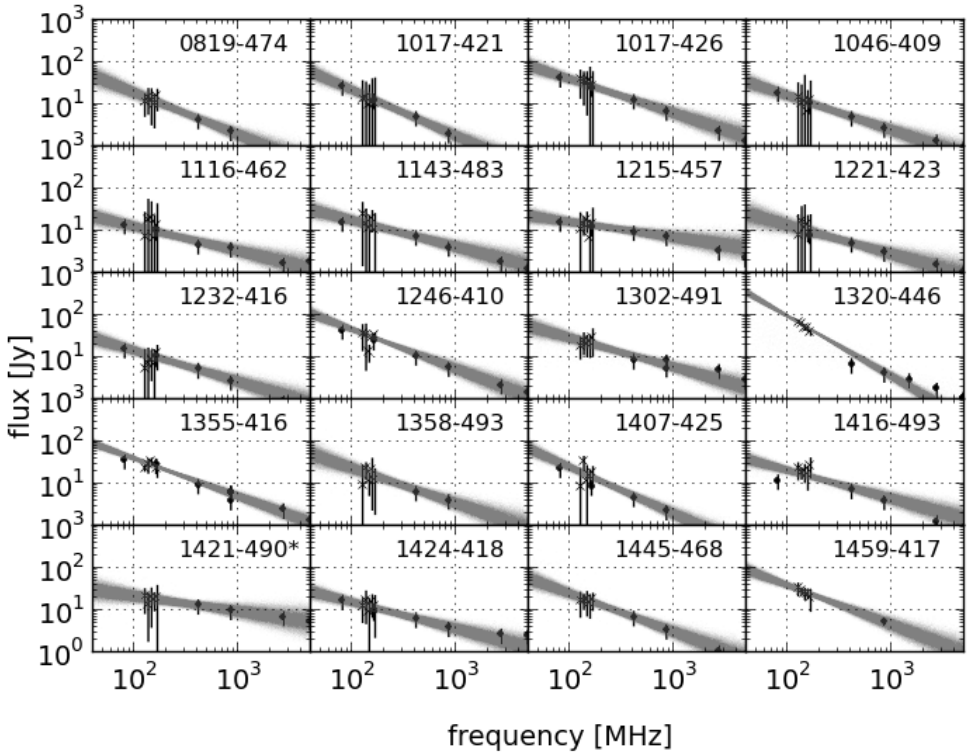

Fig. 9.— PAPER spectra of 16 sources compared against existing data out of Vollmer et al. (2010) between 40MHz and 2GHz, otherwise as described in Figure 7. Sources used to bootstrap the flux calibration are noted with a *.

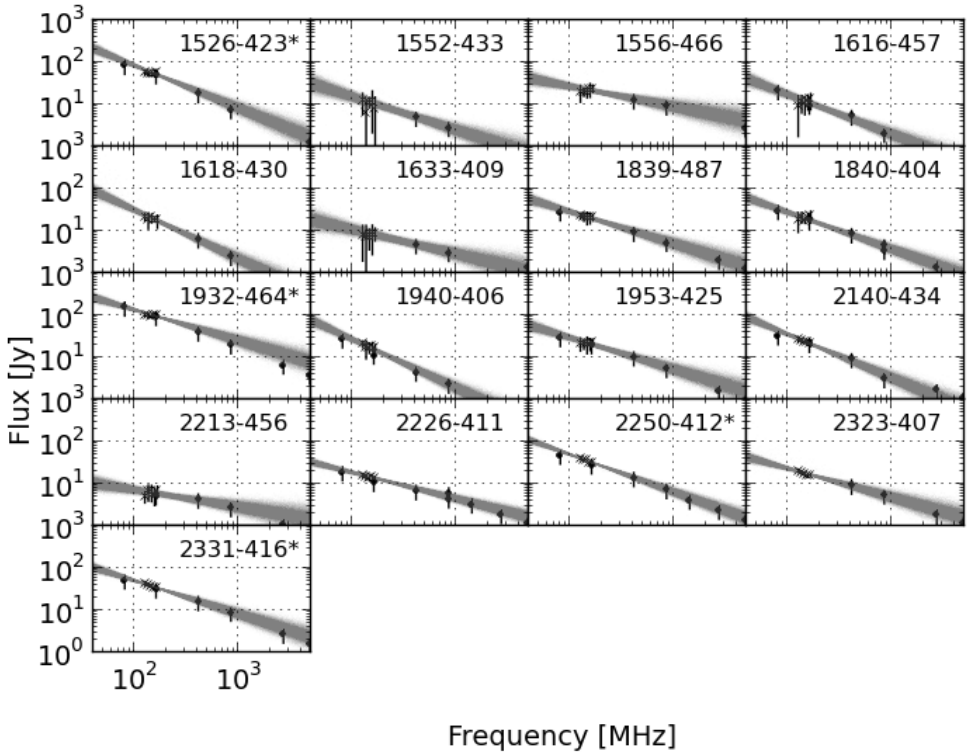

Fig. 10.— PAPER spectra of 16 sources compared against existing data out of Vollmer et al. (2010) between 40MHz and 2GHz, otherwise as described in Figure 7. Sources used to bootstrap the flux calibration are noted with a *.

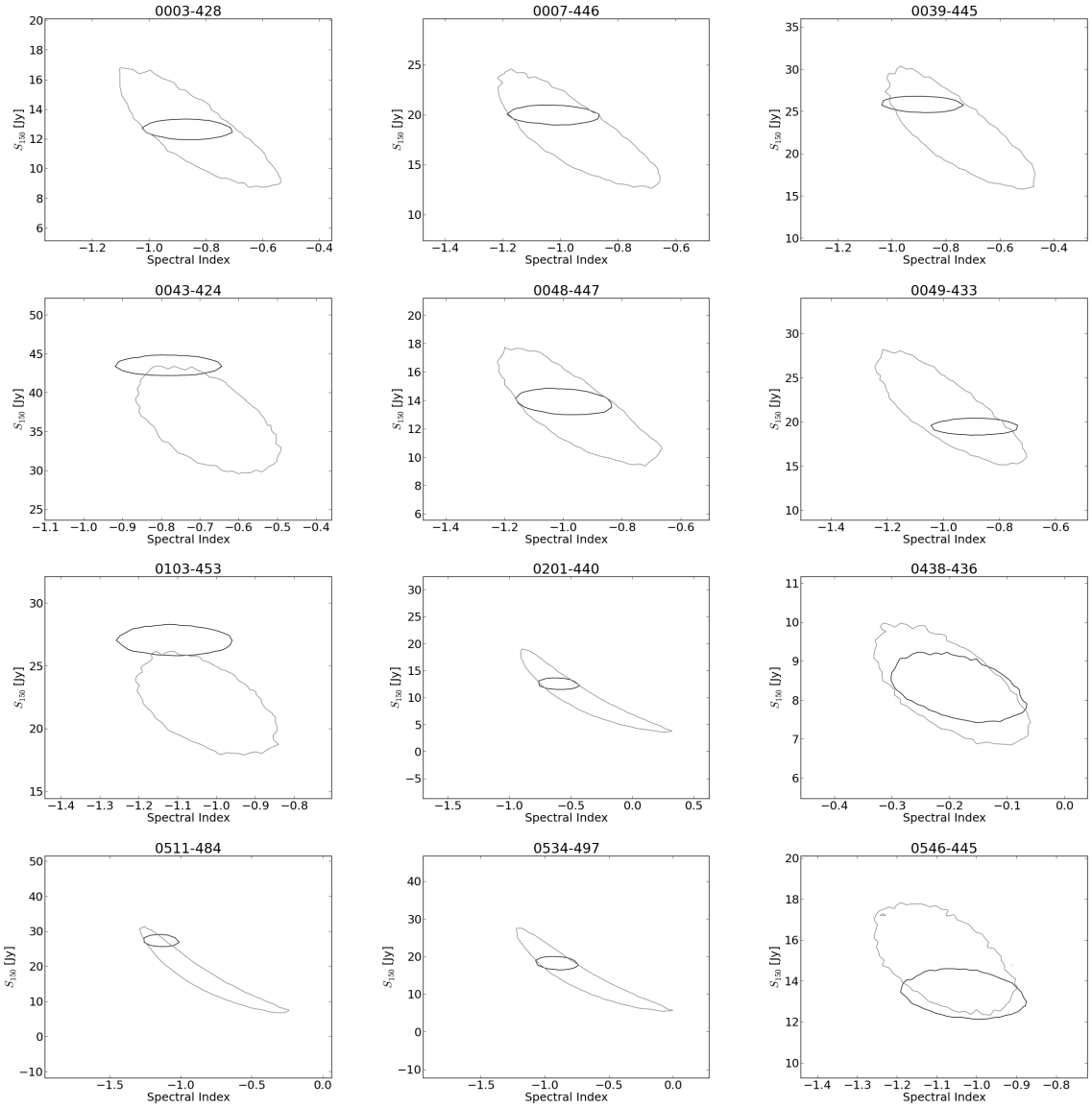

Fig. 11.— Spectral model contours as described in Figure 7. Sources marked with a * were used to assess calibration error.

2

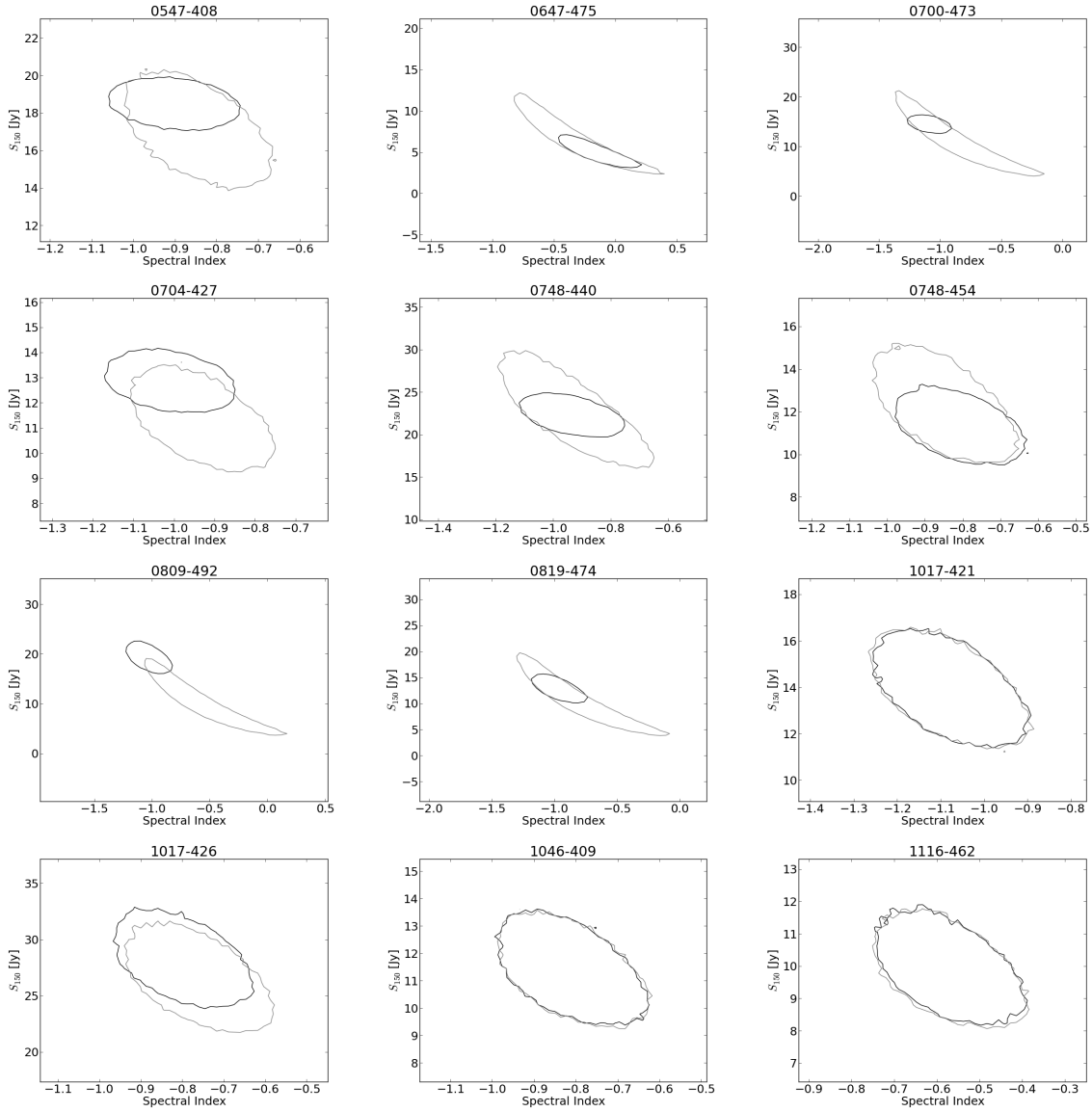

Fig. 12.— Spectral model contours as described in Figure 7. Sources marked with a * were used to assess calibration error.

2

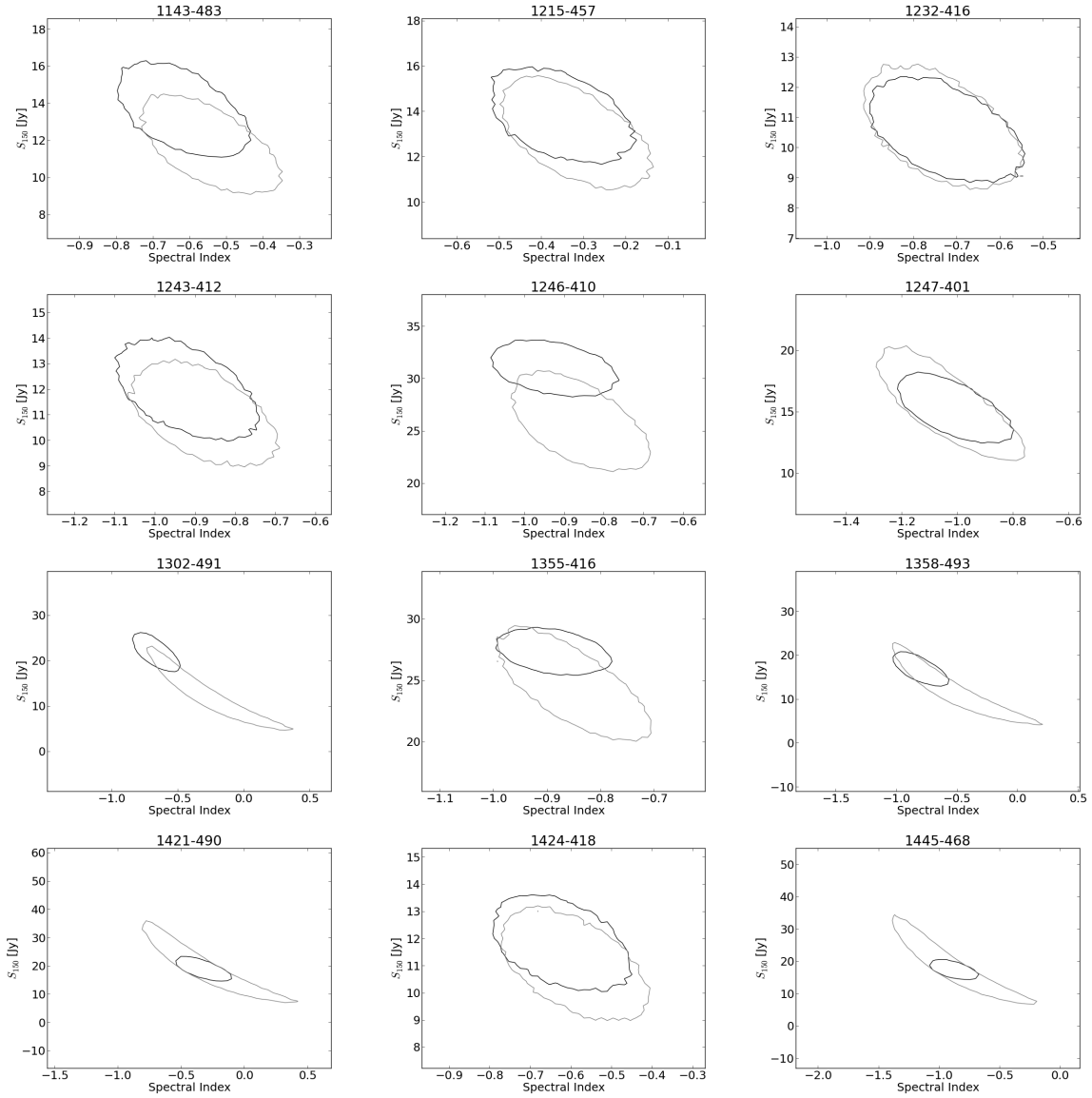

Fig. 13.— Spectral model contours as described in Figure 7. Sources marked with a * were used to assess calibration error.

2

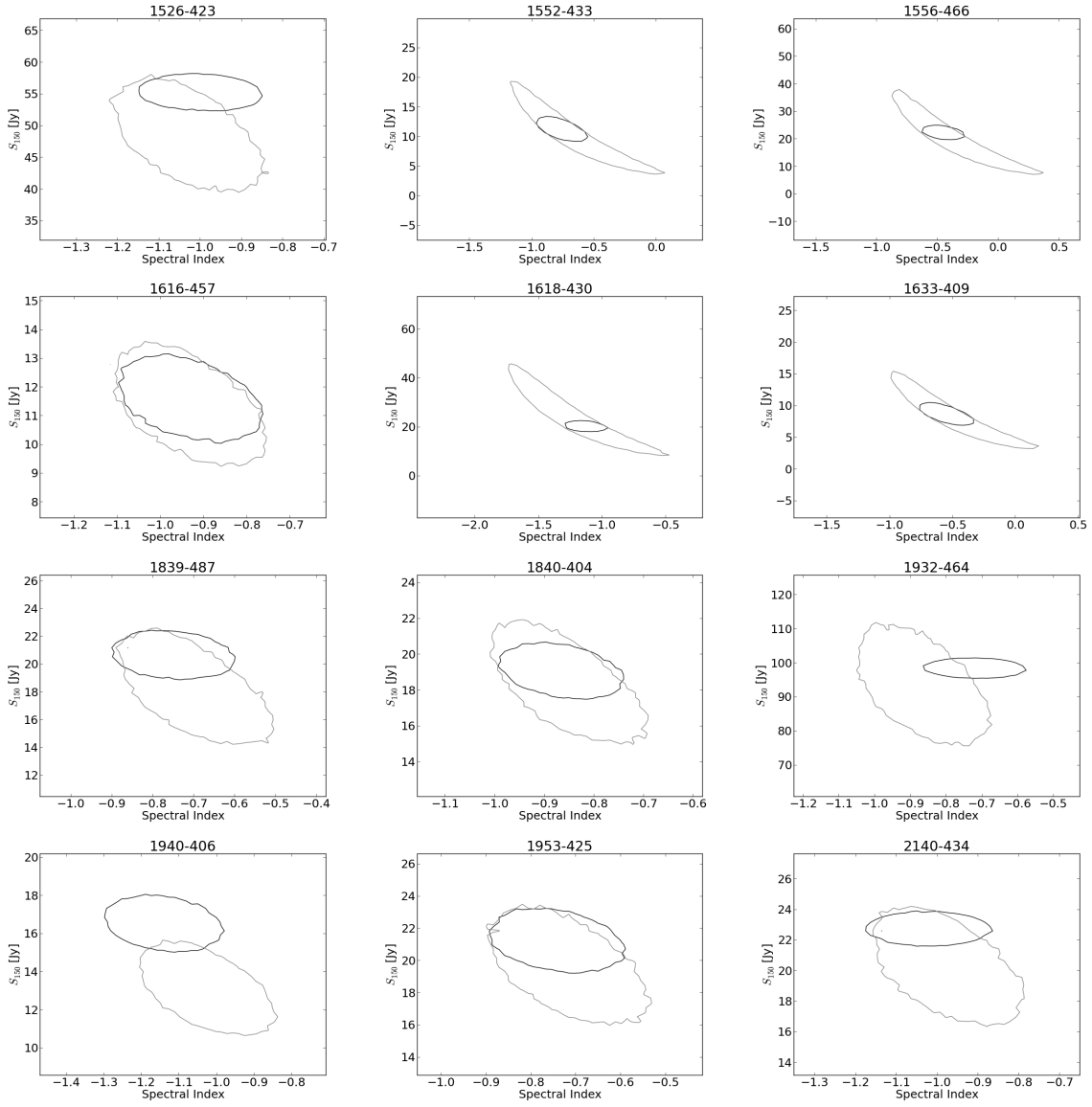

Fig. 14.— Spectral model contours as described in Figure 7. Sources marked with a * were used to assess calibration error.

2

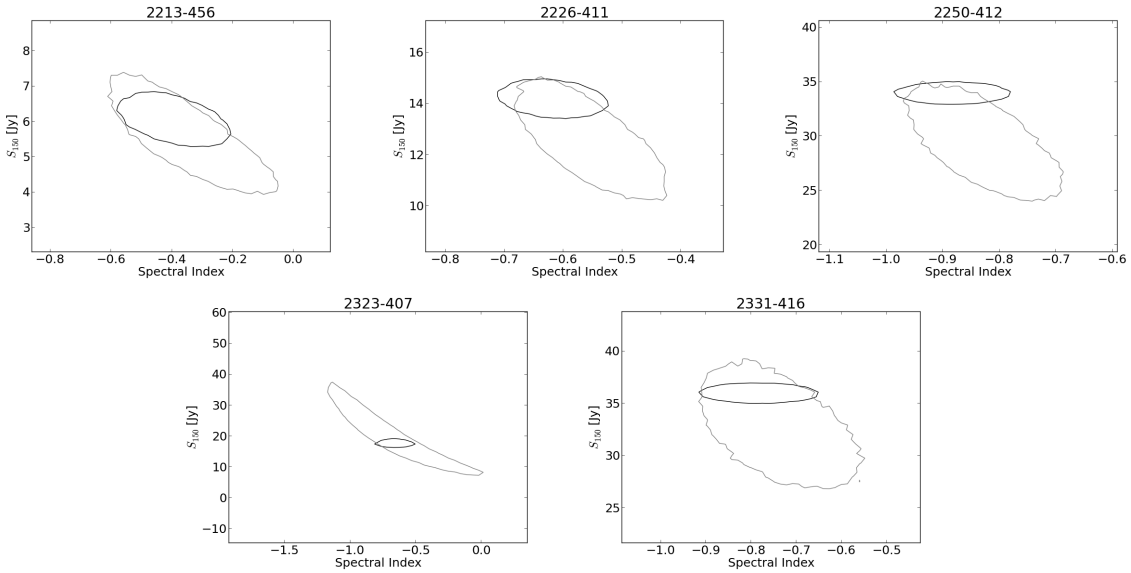

Fig. 15.— fits of the last 5 sources, as described in Figure 11. Sources marked with a * were used to assess calibration error.

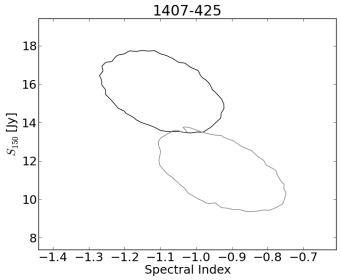

Fig. 16.— Contours of spectral fit as described in Figure 11. This source displays negative improvement. The addition of the PAPER data actually slightly increases the uncertainty.

REFERENCES

Baars, J. W. M., Genzel, R., Pauliny-Toth, I. I. K., & Witzel, A. 1977, Astronomy and Astrophysics, 61, 99, a&AA ID. AAA020.141.048

Bowman et al. 2012, PASA, submitted

Bowman, J. D. & Rogers, A. E. E. 2010, Nature, 468, 796, (c) 2010: Nature

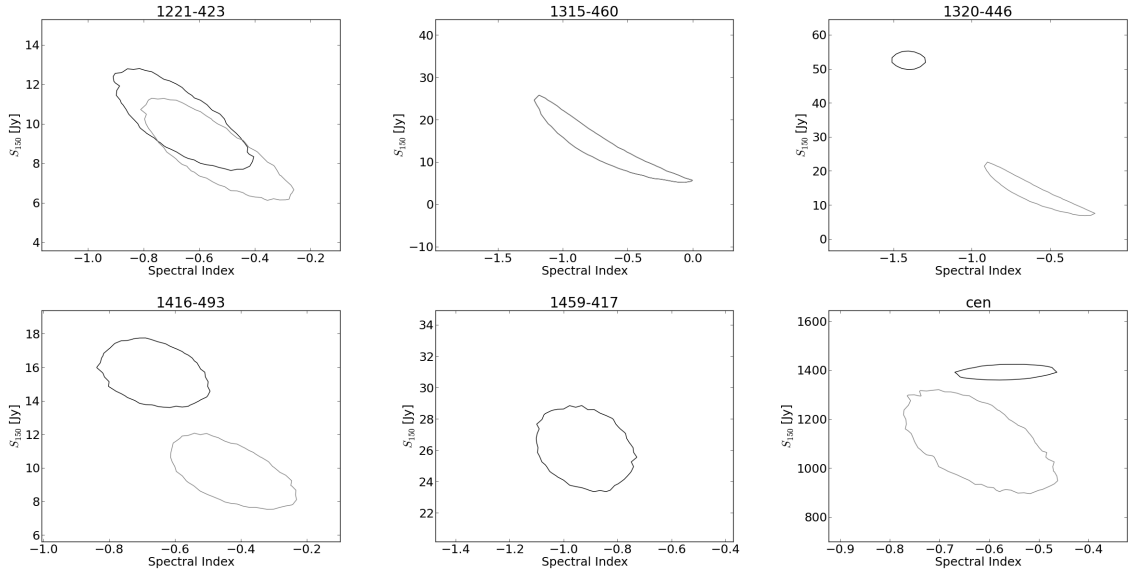

Fig. 17.— These sources are at odds with previous measurements. Two simply do not have enough prior catalog data to fit a spectral model, while the rest have suggest a deviation from the catalog spectral index fit. All are near Centaurus A (see Figure 18), a very bright, extended source, as well as the galactic plane. Side lobes manifest as ripples in the beam formed spectra which increases the error bars. See for example the Pictor A spectrum **??**. However, the sources shown here are close enough to Centaurus A that the side-lobe oscillates on scales longer than 10MHz and does not fall into the rms, but rather into the mean. Thus these few points have anomalously high fluxes and small error bars.

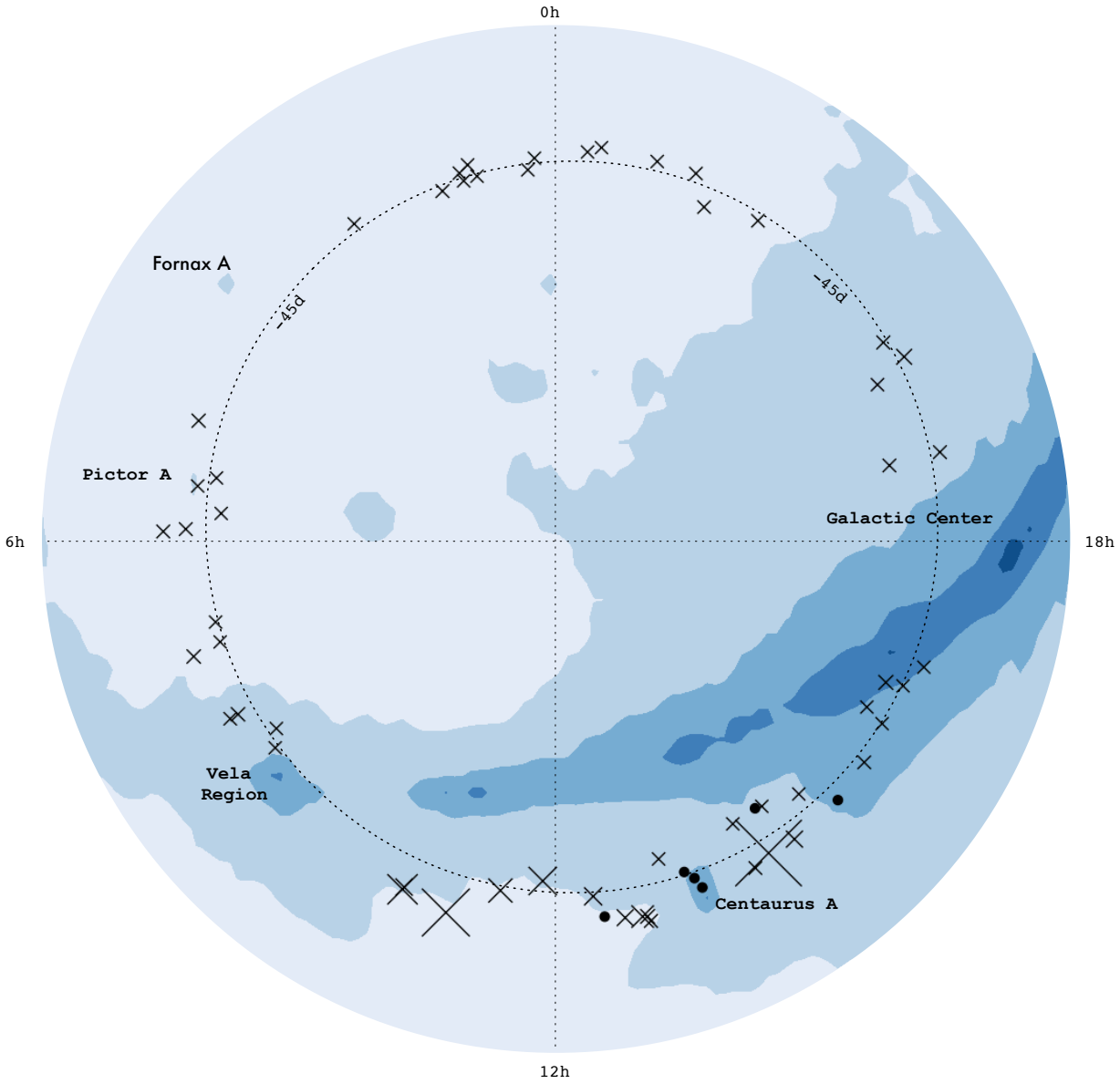

Fig. 18.— A map of the radio sky centered on the south pole (de Oliveira-Costa et al. 2008). x's mark measured locations and have size scaled by dis-agreement with prior data (inverse "improvement index" from §5). Smaller indicates better agreement with past data. Black dots indicate sources with ≤ 0 improvement score; agreement decreases with addition of PAPER data (see Figures 16 and 17). This is most likely due to galactic, and Centaurus A, side lobes.

de Oliveira-Costa, A., Tegmark, M., Gaensler, B. M., Jonas, J., Landecker, T. L., & Reich, P. 2008, Monthly Notices of the Royal Astronomical Society, 388, 247, (c) Journal compilation © 2008 RAS

Foreman-Mackey, D., Hogg, D., Lang, D., & Goodman, J. 2012, eprint arXiv:1202.3665

Furlanetto, S. R., Oh, S. P., & Briggs, F. H. 2006, Physics Reports, 433, 181, elsevier B.V.

Hogg, D. W., Bovy, J., & Lang, D. 2010, eprint arXiv, 1008, 4686, a chapter from a non-existent book

Jacobs, D. et al. 2011, The Astrophysical Journal, 734, L34

Jacobs, D., Bowman, J., & Aguirre, J. 2013, arXiv, astro-ph.CO, 10 pages, 10 figures, submitted to ApJ

Kuehr, H., Witzel, A., Pauliny-Toth, I., & Nauber, U. 1981, Astronomy and Astrophysics Supplement Series, 45, 367

Large, M. I., Mills, B. Y., Little, A. G., Crawford, D. F., & Sutton, J. M. 1981, ROYAL ASTRON. SOC. MONTHLY NOTICES V.194, 194, 693, a&AA ID. AAA029.002.002

Mackay, D. J. C. 2003, Information Theory

Morales, M. F. & Wyithe, J. S. B. 2010, Annual review of astronomy and astrophysics, 48, 127

Offringa, A. R., de Bruyn, A. G., & Zaroubi, S. 2012, Monthly Notices of the Royal Astronomical Society, 422, 563

Otrupcek, R. & Wright, A. 1991, Proceedings of the Astronomical Society of Australia, 9, 170

Paciga, G. et al. 2013, eprint arXiv:1301.5906

—. 2011, Monthly Notices of the Royal Astronomical Society, 413, 1174

Parsons, A. et al. 2010, The Astronomical Journal, 139, 1468

Parsons, A. R. & Backer, D. C. 2009, The Astronomical Journal, 138, 219

Perley, R. A., Roser, H.-J., & Meisenheimer, K. 1997, Astronomy and Astrophysics, 328, 12

Pober, J. C. et al. 2013, eprint arXiv, 1301, 7099, 6 pages, 5 figures, submitted to ApJL

—. 2012, The Astronomical Journal, 143, 53

Press, W. 1997, Unsolved Problems in Astrophysics, 49

Pritchard, J. R. & Loeb, A. 2012, Reports on Progress in Physics, 75, 6901

Sivia, D. & Skilling, J. 2006, citeulike.org

Slee, O. 1995, Australian Journal of Physics, 48, 143, d

Stefan, I. I. et al. 2012, eprint arXiv, 1212, 1624

Tingay, S. et al. 2013, Publications of the Astronomical Society of Australia, 30, 7

Vollmer, B., Gassmann, B., Derriere, S., Boch, T., & Louys, M. 2010, arxiv.org

Williams, C. L. et al. 2012, The Astrophysical Journal, 755, 47

Wills, B. J. 1975, Australian Journal of Physics, 38, 1, a&AA ID. AAA014.141.131

Yatawatta, S. et al. 2013, Astronomy & Astrophysics, 550, 136

This preprint was prepared with the AAS LaTeX macros v5.2.

Table 1. PAPER spectra for 59 MRC sources. Full table available online

Name	Ra deg	Dec deg	S125 Jy	rms Jy	S135 Jy	rms Jy	S145 Jy	rms Jy	S155 Jy	rms Jy	S165 Jy	rms Jy
Pictor A	80.1	-45.79	459.23	30.2	416.59	28.3	397.17	21.8	375.14	18.5	359.72	17.1
0003-428	1.67	-42.5	14.98	2.0	13.45	1.2	13.02	1.8	12.9	1.6	10.42	1.2
0007-446	2.79	-44.31	23.51	2.5	21.18	2.4	20.24	1.5	18.74	1.5	17.61	1.8
0008-421	2.88	-41.81	-0.94	1.7	-0.68	1.7	0.54	1.8	0.52	1.4	1.98	1.8
0039-445	10.69	-44.16	31.95	2.9	30.29	3.0	28.54	2.1	26.0	1.9	24.06	1.4
0043-424	11.72	-42.05	51.9	4.2	47.43	3.5	45.82	2.6	42.74	3.0	40.68	2.6
0048-447	12.86	-44.41	17.86	2.6	16.02	2.3	15.15	2.5	14.51	1.5	12.51	1.6
0049-433	13.21	-43.03	23.53	2.4	21.0	1.5	21.94	2.4	20.2	1.9	18.85	2.1
0103-453	16.48	-45.02	35.5	3.2	32.61	3.5	30.86	2.4	28.21	2.5	27.2	1.5
0201-440	31.05	-43.77	16.22	4.4	15.02	1.7	13.73	1.7	12.78	1.2	14.07	1.7
0438-436	70.17	-43.53	8.44	2.5	6.26	1.9	8.05	1.6	5.74	2.1	9.0	1.7

Table 2. Spectral fits for 52 MRC sources with and without PAPER.

			PAPER[1] + Catalog				Catalog[2]			
Name	Ra	Dec	$S150$	ΔS	α	$\Delta\alpha$	$S150_p$	ΔS_p	α_p	$\Delta\alpha_p$
	deg	deg	Jy	Jy	–	–	Jy	Jy	–	–
Pictor A	80.09	-45.79	388.92	9.35	-0.77	0.02	392.08	21.36	-0.77	0.04
0003-428	1.67	-42.5	11.61	0.54	-0.81	0.03	10.32	0.76	-0.73	0.05
0007-446	2.79	-44.31	18.74	0.69	-1.0	0.03	16.98	1.26	-0.93	0.05
0039-445	10.69	-44.16	26.77	1.08	-0.92	0.11	22.71	5.1	-0.79	0.19
0043-424	11.72	-42.05	43.6	1.46	-0.79	0.11	36.16	4.97	-0.69	0.13
0048-447	12.86	-44.41	13.21	0.64	-0.98	0.04	11.58	0.88	-0.89	0.05
0049-433	13.21	-43.03	20.16	0.77	-0.97	0.03	20.54	1.53	-0.98	0.05
0103-453	16.48	-45.02	28.9	1.14	-1.16	0.11	21.76	2.93	-1.04	0.12
0201-440	31.05	-43.77	13.72	0.9	-0.71	0.12	10.31	6.54	-0.51	0.42
0438-436	70.17	-43.53	8.08	0.74	-0.19	0.09	8.32	1.09	-0.21	0.1
0511-484	78.3	-48.39	24.92	1.59	-1.14	0.09	17.3	10.7	-0.93	0.39

[1]Fits for the majority of sources (78%) that agree with prior measurements are included here. The remainder (the 6 sources shown in Figure 17) are likely contaminated by bright sources and are not included. Full table available online.

[2]MCMC fits to prior catalog data, before addition of PAPER measurements